

EXPERIMENTAL VERIFICATION OF THE MAXWELL–STEFAN FORMULATION IN DESCRIBING COMPOSITION TRAJECTORIES DURING AZEOTROPIC DISTILLATION

P. A. M. SPRINGER, S. VAN DER MOLEN, R. BAUR and R. KRISHNA

Department of Chemical Engineering, University of Amsterdam, Amsterdam, The Netherlands

Experiments were carried out in a bubble cap distillation column operated at total reflux with the quaternary mixture: water (1)–ethanol (2)–methanol (3)–acetone (4). This system has a binary minimum-boiling azeotrope for the water–ethanol mixture and the distillation boundary is represented by a surface with its corners at pure acetone, pure methanol and the water–ethanol azeotrope. For certain starting compositions the measured distillation composition trajectories clearly demonstrate that crossing of the distillation boundary is possible. In order to rationalize the experimental results, the authors develop a rigorous nonequilibrium (NEQ) stage model, incorporating the Maxwell–Stefan diffusion equations to describe transfer in either fluid phase. The developed NEQ model anticipates the boundary crossing effects, and is in excellent agreement with a series of experiments. In sharp contrast, an equilibrium (EQ) stage model fails even at the *qualitative* level to model the experiments. The differences in the NEQ and EQ trajectories emanates from differences in the component Murphree efficiencies, which in turn can be traced to differences in the binary pair vapour phase diffusivities. It is concluded that for reliable design of azeotropic distillation columns interphase mass transfer effects must be taken into account in a rigorous manner.

Keywords: quaternary azeotropic distillation; Maxwell–Stefan equations; distillation surface; nonequilibrium stage; equilibrium stage.

INTRODUCTION

Most commercially available simulation programs for distillation columns cater for ‘real’ or non-equilibrium trays¹. The departure of these real trays from equilibrium behaviour is allowed for in either of two ways. In the first procedure, the user is allowed to specify the individual component Murphree efficiencies for each stage. These component efficiencies can be estimated ‘off-line’ by using the various mass transfer correlations^{2–6} as discussed in the standard texts on distillation^{1,7,8}. The second approach, which is gaining favour, is to use a fully rate-based approach. In this approach, the interphase mass and heat transfer equations are solved simultaneously along with the interphase equilibrium relations for each stage^{9–13}. In the rate-based approaches, the interphase mass transfer relations are invariably based on the Maxwell–Stefan diffusion equations in either fluid phase^{13–15}. The rate based approach has been applied in recent times to simulate various complex flow patterns on distillation trays^{16,17} and to model maldistribution in packed distillation towers¹⁸. The rate based approach has also been extended to include three-phase distillation¹⁹, sour-gas absorption²⁰, and reactive distillation²¹.

There is some evidence in the published literature that experimentally measured composition profiles in distillation columns are better simulated with models based

on the rigorous Maxwell–Stefan diffusion equations than with simpler models that assume equal component efficiencies^{13,14,22–26}. Of particular interest and significance are the experimental measurements of Pelkonen *et al.*^{24,25} and Springer *et al.*²⁶. Pelkonen *et al.*²⁴ performed total reflux experiments with the system methanol–iso-propanol–water in a *packed* distillation column and showed that if the composition at the top of the column is located close to the distillation boundary (i.e. the line connecting pure methanol with the methanol–iso-propanol binary azeotrope) the experimentally measured composition profiles end up with a reboiler composition that is rich in water. The measured composition trajectories can be simulated very well using a nonequilibrium (NEQ) stage model incorporating the Maxwell–Stefan diffusion equations. On the other hand, an equilibrium (EQ) stage model (i.e. a model in which the component efficiencies are each taken to 100%) predicts that the reboiler composition corresponds to pure iso-propanol. Differences in the component efficiencies cause the deviation in the NEQ and EQ column trajectories^{22,23}. Pelkonen *et al.*^{24,25} also performed similar experiments with the quaternary system acetone–methanol–iso-propanol–water, with the composition near the top of the column chosen to lie on the distillation boundary, and obtained the same dramatic differences between the predictions of the EQ and NEQ models. The NEQ model predictions were in accord with experiments.

The experimental results of Springer *et al.*²⁶ with the ternary azeotropic system ethanol–water–acetone in a bubble cap tray column show that even straight line boundaries can be crossed; this boundary crossing phenomena is anticipated by the NEQ model but not by the EQ model.

The major objective of this paper is to extend the authors earlier work²⁶ and to demonstrate that for *quaternary* azeotropic distillation in a tray column, distillation boundaries (which are surfaces dividing the composition space into two regions) can be crossed as well, provided that the starting compositions are located within a finite region of compositions on one side of the boundary. Furthermore, the paper aims to show that such boundary crossing phenomena can be predicted by NEQ models, incorporating the Maxwell–Stefan equations and can be attributed to differences in component Murphree efficiencies. Clearly, the EQ models will be incapable of anticipating boundary crossing effects since the EQ distillation trajectories must necessarily follow the residue curve lines for total reflux operations^{8,27}.

To verify the boundary crossing phenomena, the authors performed experiments with the quaternary system: water (1)–ethanol (2)–methanol (3)–acetone (4) in a bubble cap tray distillation column. The vapour–liquid equilibrium was determined using NRTL parameters²⁸ and listed in Table 1. The distillation boundary forms a surface connecting the ethanol–water azeotrope with pure methanol and pure acetone. The distillation boundary (surface) is shown in Figures 1(a), (b) and (c), that represent three different views of the quaternary composition space. Consider Figures 1(a) and (b), the three dimensional composition space is viewed from two different sides; Figure 1(a) shows the component methanol in front whereas Figure 1(b) shows the component acetone in front. If only the front of these two projections is considered (the component at the back is set to zero), the projections of the ternary systems: water–ethanol–methanol (Figure 1(d)) and water–ethanol–acetone (Figure 1(e)) remain respectively with their own distillation boundaries (called: the ‘methanol boundary’ in 1(d) and the ‘acetone boundary’ in 1(e)). In Figure 1(f), the two distillation boundaries (Figure 1(d,e)) are combined together with all the ‘pseudo distillation boundary-lines’ that lie in between (represented by the gray shaded region); only when a point is located below this shaded region, you can be sure that the point is actually lying below the distillation boundary surface. Figure 1(g) shows the same graph as Figure 1(f), but with a different axis-arrangement.

EXPERIMENTAL SET-UP

The experiments were carried out in a laboratory-scale distillation column supplied by Schott Nederland B V (see Figure 2). The double layered glass column with vacuum between the inner and outer shell contains a total condenser (stage 1), a partial reboiler (stage 12) and ten equal bubble cap trays (stages 2 to 11) for which the dimensions are tabulated in Table 2 and pictured in the inset to Figure 2. The distillation column is divided into two sets of five bubble cap trays by an intersection at which a continuous feed can be introduced to the column. Product streams can be tapped automatically from the condenser and manually from the reboiler. The glass distillation column has several small openings of 10 mm in diameter, which are sealed with Teflon-coated septums. These openings enable liquid and vapour samples to be withdrawn by means of a syringe. The column has a total height of 2160 mm and a 50 mm inner diameter.

The reboiler is placed in a heating mantle, which is connected with a PC provided with the required software (Honeywell: WinNT-workstation 4.0; FIX MMI V 6.15/75-I/O-points runtime; OPTO CONTROL rel.2.2a). By means of the PC, the reboiler temperature can be controlled as well as the feed- and product-flows. Furthermore, it provides an automatic safety shut down in case the column reboiler accidentally tends to dry up. The condenser is connected with a water tap, which supplies cooling water to the glass cooling tubes inside the condenser.

Experiments under total reflux conditions and atmospheric pressure were carried out with the quaternary system water–ethanol–methanol–acetone. For any given experiment, 9 vapour and 4 liquid samples were taken from several stages (see Figure 2) and the temperature profile was measured with Pt 100 sensors. Each sample volume was intentionally kept small (100 μ L) to prevent changes in the composition-profile during the entire experiment. The samples were first dissolved into a reference solvent consisting of 1 vol% cyclohexane in 99 vol% *n*-propanol before injection into the Gas Chromatograph (type: GC8000-Top with pressure/flow control) by means of an autosampler (type AS800). The channel inside the GC is made of stainless steel and has a total length of 1 m and 0.3175 mm diameter. The carrier gas used was Helium because of its high thermal conductivity and chemical inertness. By analyzing samples of pre-prepared, known, compositions, the GC was carefully calibrated. More detailed descriptions of the experimental set-up, measurement technique, GC analysis and composition determination, including pictures

Table 1. NRTL parameters for binary mixtures at 101.3 kPa, taken from Gmehling and Onken²⁸. These parameters are used along with $G_{ij} = \exp(-\alpha_{ij}\tau_{ij})$ and $\tau_{ij} = B_{ij}/T$.

Component <i>i</i>	Component <i>j</i>	$B_{ij}/[K]$	$B_{ji}/[K]$	$\alpha_{ij}/[-]$
Water	Ethanol	624.92	-29.17	0.294
Water	Methanol	594.63	-182.61	0.297
Water	Acetone	602.63	330.48	0.510
Ethanol	Methanol	73.41	-79.17	0.303
Ethanol	Acetone	188.90	22.83	0.301
Methanol	Acetone	97.78	107.83	0.301

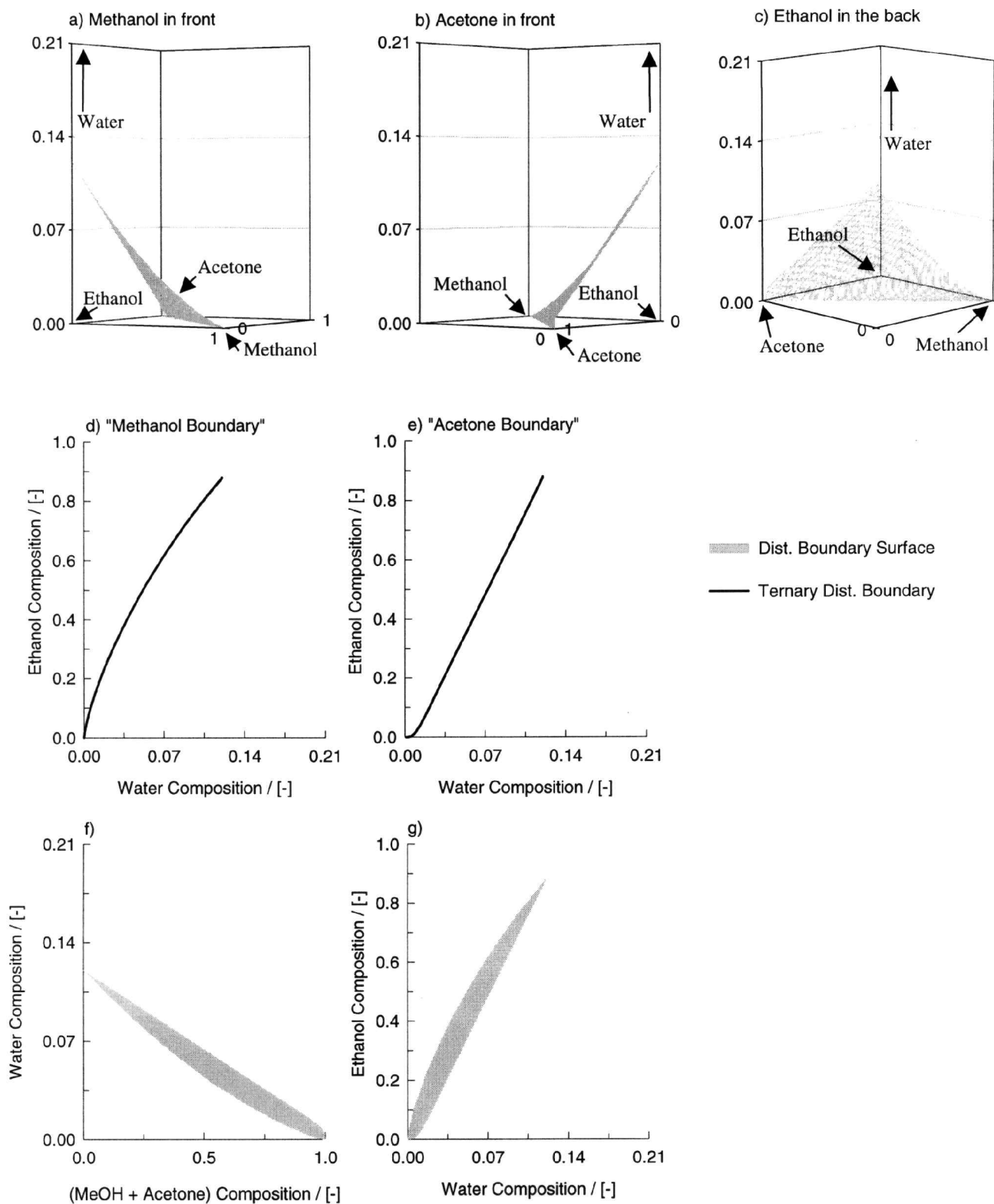


Figure 1. (a-b-c). Three dimensional residue curve space for the water (1)–ethanol (2)–methanol (3)–acetone (4) system, showing an almost plane distillation boundary-surface with its corners at pure methanol, pure acetone and the binary azeotrope between water–ethanol. (d) Front view projection of Figure 2(a) with the methanol component in front, showing the ternary 'methanol boundary'. (e) Front view projection of Figure 2(b) with the acetone component in front, showing the ternary acetone boundary. (f,g) Combination of the two ternary boundaries from Figure 2(d,e) together with all the 'pseudo distillation boundary-lines' that lie in between (represented by the grey shaded region).

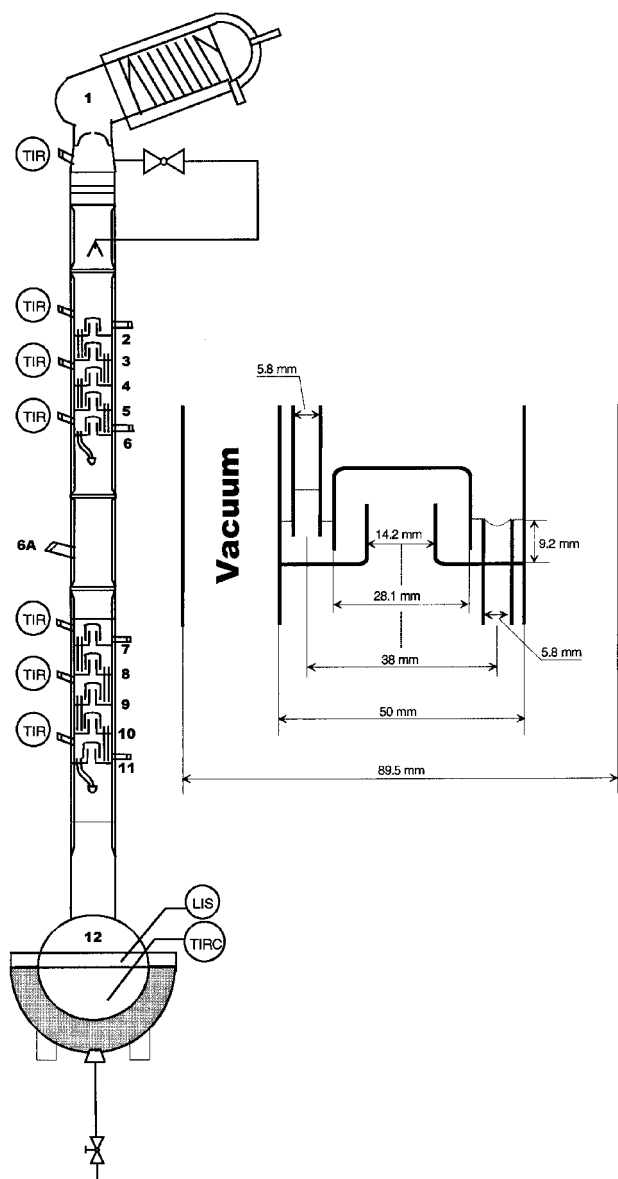


Figure 2. Schematic of laboratory-scale distillation column. Includes total condenser (1), partial reboiler (12), ten bubble cap trays (2–11) and 13 draw-off faucets, 9 for vapour samples (V) and 4 for liquid samples (L). The details of the bubble cap are shown on the right side of the column.

Table 2. Bubble cap tray design of the laboratory-scale distillation column.

Column diameter	50 mm	Hole pitch	14.2 mm
Tray spacing	46.2 mm	Cap diameter	28.1 mm
Number of flow passes	1	Skirt clearance	3 mm
Liquid flow path length	30.8 mm	Slot height	5 mm
Downcomer clearance	3.9 mm	Active area (of total area)	97.30%
Deck thickness	3 mm	Total hole area (of total area)	8.27%
Hole diameter	14.2 mm	Downcomer area (of total area)	1.35%
Weir type	Circular	Slot area	221 mm ²
Weir length	18.2 mm	Riser area	158 mm ²
Weir height	9.2 mm	Annular area	462 mm ²
Weir diameter	5.8 mm		

of the column and bubble cap trays are available on the authors' web-site: <http://ct-cr4.chem.uva.nl/distillation/>.

EXPERIMENTAL RESULTS

The experimentally determined composition trajectories for a set of six experiments are presented in Figure 3(a)–(f) in three different projections for each single experiment. The first two projections of Figure 3(a)–(f) are similar to the projections shown in Figure 1(d) and 1(e). The third projection is obtained when looking at the distillation boundary surface from above with the component ethanol at the rear (as in Figure 1(c)). This projection does not give any information concerning a possible boundary crossing, but does show from another point of view, the differences between the trajectories predicted by the EQ model versus NEQ model, to be discussed and developed below. At total reflux the composition of the vapour leaving any given stage equals the composition of the liquid arriving at that stage from above. Therefore, the 9 vapour and 4 liquid composition samples can be combined when plotting the composition trajectories. In Figure 3, the vapour samples are denoted by open circles and the liquid samples by open squares. In experiment Q1, the column trajectory was located completely below the distillation boundary surface, which corresponds to the left of the ternary distillation boundaries in Figure 3(a-1) and 3(a-2) (indicated by a thick line). All the remaining five experiments, Q2 to Q6, clearly exhibit boundary crossing phenomena. In these experiments both the 'methanol' and 'acetone' boundaries are crossed. Clearly, boundary crossing phenomena is not in conformity with the assumption of thermodynamic phase equilibrium; this is evidenced by the fact that the experimental trajectories do not agree with the constraints, enforced by the distillation boundary (surface). In order to understand, and rationalize, the boundary crossing phenomena a rigorous nonequilibrium (NEQ) stage model is developed.

NONEQUILIBRIUM STAGE MODEL DEVELOPMENT

The development of the NEQ stage model follows the ideas and concepts developed earlier by Taylor, Krishna and others and described in earlier publications^{9–15,22,23,26}. A brief review of the model development for a *quaternary* mixture is given below. Consider first a single stage pictured in Figure 4. All the authors, experiments were carried out in the bubbly flow regime. In the model development the authors assumed that the bubbles rise through the liquid in a plug flow manner. Furthermore, it was assumed that the liquid phase was well-mixed. The steady state component molar balance for 4-component distillation in tray columns is given by the 3-dimensional matrix relation:

$$V_b = \frac{d(y)}{dh} = [K_{Oy}](y^* - y)a' \quad (1)$$

where a' is the interfacial area per unit volume of the dispersed bubble phase and V_b is the bubble rise velocity. Equation (1) can be re-written in terms of the overall number of transfer units for the vapour phase $[NTU_{Oy}]$:

$$\frac{dy}{d\zeta} = [NTU_{Oy}](y^* - y) \quad (2)$$

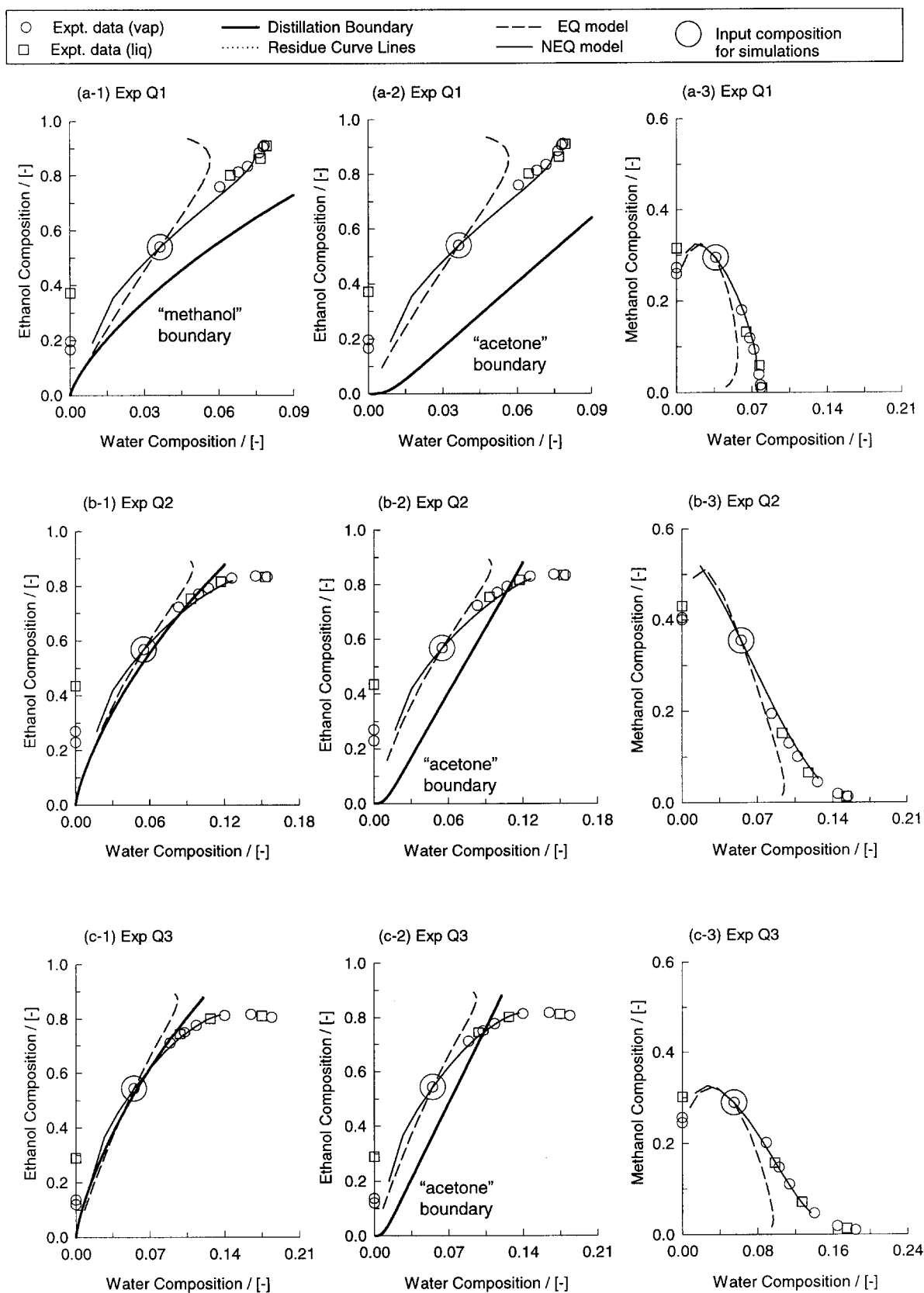


Figure 3. (a)–(c) are the results of experiments Q1–Q3 (open circles for vapour samples and open squares for liquid samples) showing the column composition trajectories for the water (1)–ethanol (2)–methanol (3)–acetone (4) system in three different front view projections. Also shown are the simulation results showing the trajectories calculated by the equilibrium (EQ) stage model and the nonequilibrium (NEQ) stage model. The large open circles represent the experimental composition used as input in the simulations. In the NEQ model simulations a bubble size $d_b = 5.0$ mm was chosen. (d)–(f) are the results of experiments Q4–Q6. Other specifications are the same as (a)–(c).

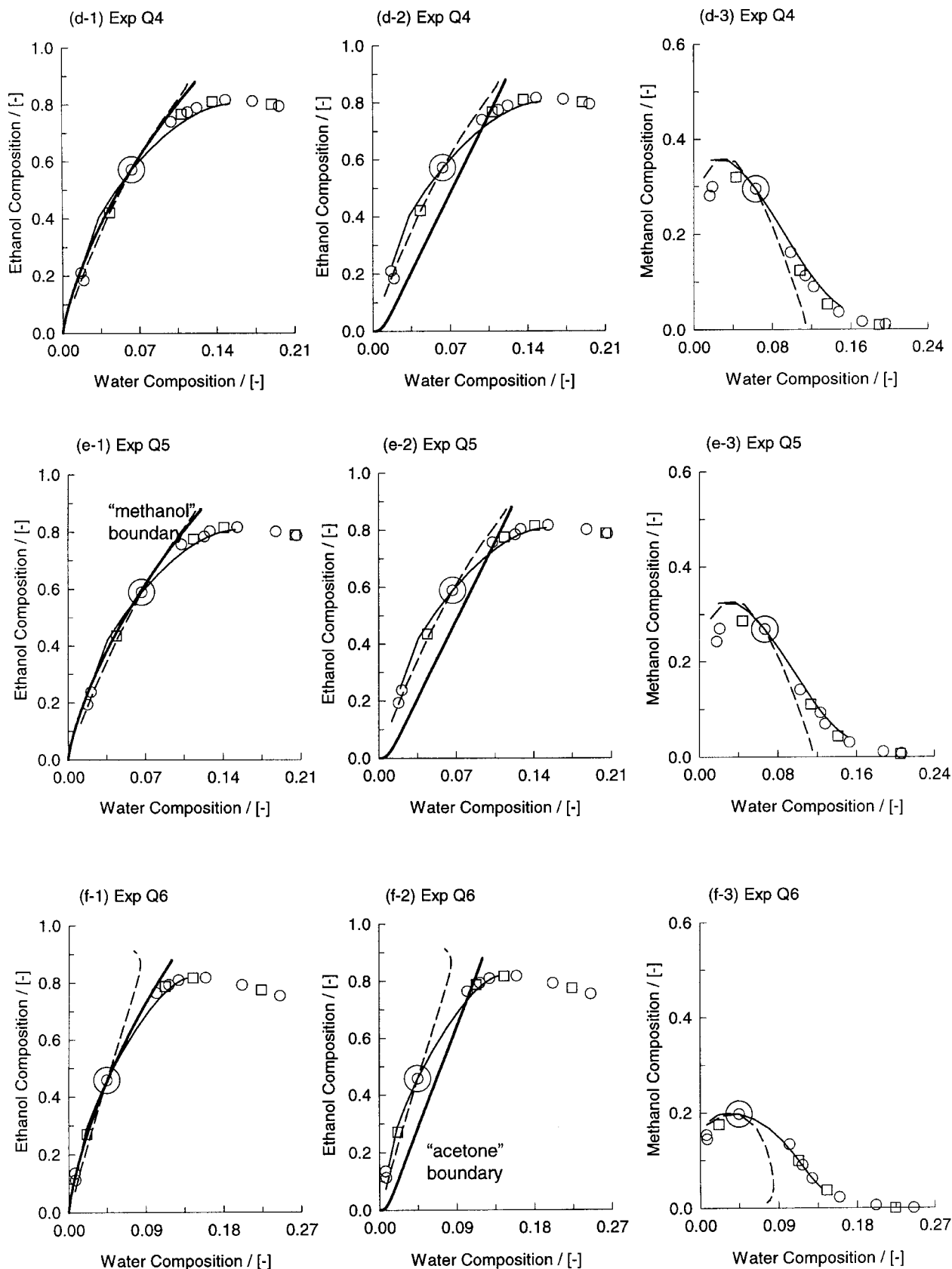


Figure 3. Continued

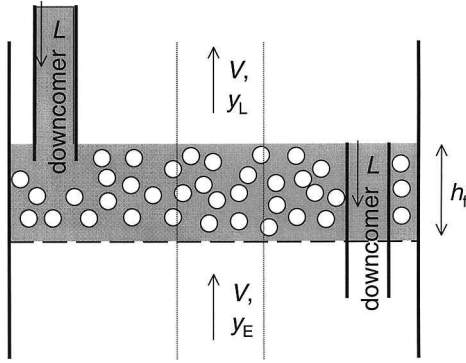


Figure 4. Schematic of the bubble froth regime on the tray.

where $\xi = h/h_f$ is the dimensional distance along the froth and $[NTU_{Oy}]$ is defined as:

$$[NTU_{Oy}] \equiv \int_0^{h_f} [[K_{Oy}]a'/V_b] dh \quad (3)$$

Carrying out the integration, assuming that the matrix of overall mass transfer coefficients $[K_{Oy}]$ does not vary along the froth height, gives:

$$[NTU_{Oy}] \equiv [K_{Oy}]a'h_f/V_b \equiv [K_{Oy}]a'\tau_v \quad (4)$$

From equation (4), it can be seen that $[NTU_{Oy}]$ can be calculated from knowledge of $[K_{Oy}]$, the interfacial area per unit volume of vapour a' and the vapour phase residence time τ_v . In the authors' model, it was assumed that all the bubbles were spherical in shape with a diameter d_b . The interfacial area per unit volume of vapour a' is, therefore, given by:

$$a' = \frac{6}{d_b} \quad (5)$$

The vapour residence time is determined by:

$$\tau_v = \frac{h_f}{V_b} \quad (6)$$

where h_f is the height of dispersion (froth); this is taken to be the height of the downcomer tube above the tray floor, i.e. 9.2 mm as seen in Figure 2. The bubble rise velocity V_b is estimated using the Mendelson equation²⁹, recommended by Krishna *et al.*³⁰:

$$V_b = \sqrt{\frac{2\sigma}{\rho_L d_b} + \frac{g d_b}{2}} \quad (7)$$

The overall matrix of mass transfer coefficients $[K_{Oy}]$ is given by the addition of resistances formula:

$$[K_{Oy}]^{-1} = [k_y]^{-1} + \frac{c_L^V}{c_L^L} [K_{eq}] [k_x]^{-1} \quad (8)$$

in which $[K_{eq}]$ represents the diagonal matrix of K -values and $[k_y]$ and $[k_x]$ are the partial transfer coefficient matrices for the vapour and liquid phases respectively.

Next, consider the matrix of the multicomponent vapour mass transfer coefficient $[k_y]$. The nine elements $k_{y,ij}$ can be

estimated from the mass transfer coefficients of the constituent binary pairs, $\kappa_{y,ij}$ from:

$$[k_y] = [R_y]^{-1} \quad (9)$$

where the elements of the matrix of inverse mass transfer coefficients $[R_y]$ is given by:

$$R_{y,ii} = \frac{y_i}{\kappa_{y,in}} + \sum_{k \neq i}^4 \frac{y_k}{\kappa_{y,in}};$$

$$R_{y,ij} = -y_i \left(\frac{1}{\kappa_{y,ij}} - \frac{1}{\kappa_{y,in}} \right); \quad i = 1, 2, 3 \quad (10)$$

For each of the binary pairs in the mixture, the $\kappa_{y,ij}$ can be estimated from the following equation for instationary diffusion within a spherical bubble¹³:

$$Sh_{ij} \equiv \frac{\kappa_{y,ij} d_b}{D_{y,ij}} = \frac{2}{3} \pi^2 \left(\frac{\sum_{m=1}^{\infty} \exp\{-m^2 \pi^2 Fo_{ij}\}}{\sum_{m=1}^{\infty} 1/m^2 \exp\{-m^2 \pi^2 Fo_{ij}\}} \right) \quad (11)$$

with $ij = 12, 13, 14, 23, 24, 34$. For Fourier numbers $Fo_{ij} \equiv 4D_{y,ij}\tau_v/d_b^2$ larger than 0.06, the Sherwood number reduces to the asymptotic value:

$$Sh_{ij} = \frac{2\pi^2}{3} \approx 6.58; \quad ij = 12, 13, 14, 23, 24, 34 \quad (12)$$

For this steady-state limit, the binary vapour mass transfer coefficients are given by:

$$\kappa_{y,ij} = \frac{2\pi^2 D_{y,ij}}{3 d_b}; \quad ij = 12, 13, 14, 23, 24, 34 \quad (13)$$

Equation (13) leads to the important conclusion that $\kappa_{y,ij}$ would have an unity-power dependence on the vapour diffusivity $D_{y,ij}$, which is in sharp contrast with the square-root dependence for small values of Fo , i.e. small vapour phase residence times.

The matrix of the multicomponent liquid mass transfer coefficient $[k_x]$ can be obtained analogously to equations (9)–(10). The binary liquid mass transfer coefficient $\kappa_{x,ij}$ can be obtained from the penetration model:

$$\kappa_{x,ij} = 2 \sqrt{\frac{D_{x,ij}}{\pi t_c}}; \quad ij = 12, 13, 14, 23, 24, 34 \quad (14)$$

where the contact time of the liquid with gas bubbles, t_c is given by:

$$t_c = \frac{d_b}{V_b} \quad (15)$$

In the above set of model equations, the only unknown parameter is the bubble diameter d_b . Once the bubble diameter is set, the system of equations can be solved. Substituting equation (8) into equation (4) gives the $[NTU_{Oy}]$. Assuming that the $[NTU_{Oy}]$ on a single stage is constant, equation (2) can be integrated using the boundary conditions:

$$\xi = 0 \text{ (inlet to tray)} \quad (y) = (y_E)$$

$$\xi = 1 \text{ (outlet of tray)} \quad (y) = (y_L) \quad (16)$$

to obtain the compositions leaving the distillation stage (detailed derivations are available in reference¹³):

$$(y^* - y_L) = \exp[-[NTU_{Ov}]](y^* - y_E) \quad (17)$$

Introducing the matrix $[Q] \equiv \exp[-[NTU_{Ov}]]$, equation (17) may be rewritten in the form:

$$(y_L - y_E) = [[I] - [Q]](y^* - y_E) \quad (18)$$

where $[I]$ is the identity matrix. The limiting case of the EQ stage model is obtained when the mass transfer coefficients in either fluid phase attain large values; $[Q]$ reduces in this case to the null matrix and the compositions leaving the tray (y_L) are equal to (y^*), in equilibrium with the liquid leaving the tray.

The material balance relations outlined above need to be solved along with the enthalpy balance relations, as described in Chapter 14 of Taylor and Krishna¹³. The required heat transfer coefficients in the vapour phase are calculated from the heat transfer analog of equation (11) for the vapour phase Nusselt number. Similarly, the liquid phase heat transfer coefficient is obtained by the application of the penetration model to the liquid phase, analogous to equation (14). The entire set of material and energy balance equations, along with the interphase mass and energy transfer rate relations are then incorporated into a rigorous stage-to-stage model as described in Chapter 14 of Taylor and Krishna¹³. This chapter contains more exhaustive details of this model including sample calculations for binary and ternary mixtures.

SIMULATION STRATEGY

Simulations of the total reflux experimental runs were carried out using both the equilibrium (EQ) stage model and the rigorous nonequilibrium stage (NEQ) stage model developed above. The operating pressure for all experiments was 101.3 kPa and the ideal gas law was used. Activity coefficients were calculated using the NRTL interaction parameters, specified in Table 1, and the vapour pressures were calculated using the Antoine equations. The vapour phase was assumed to be thermodynamically ideal. The column consists of 12 stages, including the total condenser (stage 1) and partial reboiler (stage 12). The reflux flow rate (0.006 mol s^{-1}) and the bottom flow rate (0.0 mol s^{-1}) were used for specifying the column-operations.

Since the column is operated at total reflux, the reflux flow rate determined the inner flow rates of vapour and liquid phases on each stage. Simulation of total reflux operations is 'complicated' by the fact that there is no feed to the column at steady-state. To overcome this problem one of the experimentally determined compositions of the streams leaving or entering a stage is specified as an input parameter. The simulated composition profile of the total reflux run is forced to pass through this specified composition. In all the experiments the authors specified the vapour composition leaving stage 4 in performing the simulations. This 'input' composition is indicated by the large open circle in Figure 3. The entire set of equations system was solved numerically by using the Newton's method. The NEQ implementation is available in the software program *ChemSep*, developed by Taylor⁹⁻¹³. Detailed information on *ChemSep* are available at <http://www.chemsep.org> and in the recent book by Kooijman and Taylor¹¹; this book contains details of all thermodynamics and mass transfer models for tray columns that have been implemented into the software.

COMPARISON OF EQ AND NEQ SIMULATIONS WITH QUATERNARY EXPERIMENTS

All 6 quaternary experiments, Q1 to Q6, were simulated with both the EQ stage model and the rigorous NEQ stage model. Experiment Q6 is now considered in some detail. Figure 5(a) compares the EQ model with the experimental results. The large open circle represents the vapour composition leaving stage 4; this is specified in the simulations as 'input' composition. The authors note that while the experimental points cross the distillation boundary (grey coloured surface), the EQ column trajectory does not and remains below the boundary surface. A further point to note is that while the experimental results show that proceeding down the column (in the direction of the reboiler) the compositions get richer in water, the EQ simulations predict that these trays get progressively richer in ethanol. The NEQ model simulations require specification of the bubble diameter. The NEQ simulations were carried out for a range of bubble diameters in the 3–5.5 mm range. Decreasing the bubble diameter has the effect of increasing the mass transfer coefficient (see equations (13)–(15)) and makes the NEQ model tend towards the EQ model. To match the EQ

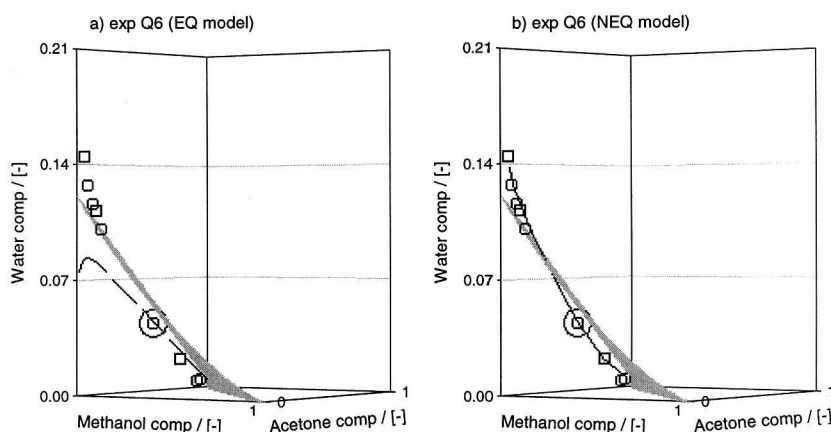


Figure 5 (a) EQ model and (b) NEQ model simulation results compared with the experimental data (open circles for vapour samples and open squares for liquid samples) for run Q6. The large open circle is the specified composition for the simulations; this corresponds to the vapour composition leaving stage 4.

trajectory, the bubble size has to be 1.5 mm, or smaller. Conversely, increasing the bubble diameter, decreases the mass transfer coefficient and the NEQ trajectories move away from the EQ trajectory. The best agreement with the experiments is obtained with $d_b = 5.0$ mm. The simulation result for the NEQ model, with $d_b = 5.0$ mm, is plotted for the experimental run Q6 in Figure 5(b). The NEQ trajectory is in very good agreement with the experiment results and is able to reproduce the boundary crossing observed.

The simulation results for the EQ and NEQ model (with $d_b = 5.0$ mm) for all the six experimental runs are shown in Figure 3(a)–(f) in three different projections, along with the experimental results.

Consider the run Q1. For this run no boundary crossing is observed experimentally; see Figure 3(a-1), (a-2) and (a-3). Both EQ and NEQ models do not anticipate boundary crossing, although the predictions of the NEQ model are superior to that of the EQ model and in much better agreement with the experimentally measured composition trajectories.

Consider the runs Q2 up to and including Q6 in Figure 3. For all these runs boundary crossing is experienced; in the experiments both the ‘methanol’ and ‘acetone’ boundaries are crossed. The NEQ model successfully anticipates the crossing of the ‘methanol’ and ‘acetone’ boundaries. In all the cases the EQ model fails to cross the ‘acetone’ boundary. For run Q2, the EQ model fails to cross the ‘methanol’ boundary as well. For all these runs the experimental results show that proceeding down the column (in the direction of the reboiler) the compositions get richer in water. The EQ simulations predict that these trays get progressively richer in ethanol; this is qualitatively different to the experimental observations.

VERIFICATION OF 5 mm BUBBLE SIZE FROM TERNARY EXPERIMENTS

To demonstrate that the choice of a 5 mm bubble size is not just a convenient fit of the quaternary experimental results, a set of nine experiments with the ternary mixture water–ethanol–methanol was also performed. The experimental results are shown in Figure 6. All experiments were simulated with the EQ stage model and the rigorous NEQ stage model, taking $d_b = 5.0$ mm. The large open circle in Figure 6 represents the vapour composition leaving stage 4; this is specified in the simulations as ‘input’.

Consider the runs T1, T2, T3 and T4. For all these runs no boundary crossing is observed experimentally. Both EQ and NEQ models do not anticipate boundary crossing. The EQ model follows the trajectory dictated by the residue curve map, whereas the NEQ model has a tendency to cut across to the right of the residue curve. The predictions of the NEQ model are superior to that of the EQ model and in much better agreement with the experimentally measured composition trajectories. This tendency of the experiments to cut across to the right of the residue curves is strongly evident for run T1, T2 and T3; here the NEQ model does a very good job of predicting the column trajectory.

Consider the runs T5, T6, T7, T8 and T9 in Figure 6. For all these runs boundary crossing is experienced and the NEQ model successfully anticipates this phenomenon. In all the cases the EQ model fails to cross the boundary and the EQ trajectory remains on one side of the boundary. For all these

runs the experimental results show that proceeding down the column (in the direction of the reboiler) the compositions get richer in water. The EQ simulations predict that these trays get progressively richer in ethanol; this is qualitatively different to the experimental observations.

COMPONENT MURPHREE EFFICIENCIES IN QUATERNARY DISTILLATION

It may be concluded from the foregoing that boundary crossing is caused by *multicomponent* mass transfer effects. To explain this in some detail consider run Q6. The values of the binary pair vapour diffusivities, $D_{y,ij}$ for water (1)–ethanol (2)–methanol (3)–acetone (4) are specified in Table 3 for stage 6, along with the corresponding liquid phase coefficients and the matrix of vapour phase transfer units $[NTU_y]$ and liquid phase transfer units $[NTU_x]$. The estimated values of the Fourier numbers calculated using:

$$Fo_{ij} = \frac{4D_{y,ij}\tau_v}{d_b^2} \quad (19)$$

also given in Table 3 for stage 6, along with the values of the surface tension (σ) and liquid density (ρ_L) that are needed in order to estimate the single bubble rise velocity (V_b) and thus the vapour residence time (τ_v). From Table 3, it can be seen that the Fo values exceed 0.06 in all cases, justifying the use of equation (12) for estimation of the vapour phase mass transfer coefficients $\kappa_{y,ij}$ of the binary pairs in the mixture; the $\kappa_{y,ij}$ have an unity-power dependence on the vapour diffusivities $D_{y,ij}$. The vapour phase diffusivities of the three binary pairs are estimated using the Fuller–Schettler–Giddings equation; details of the estimation procedure are to be found in Kooijman and Taylor¹¹; this book also specifies the estimation methods for liquid phase diffusivities, densities and surface tension. By evaluating the individual contributions of the liquid and vapour phases in equation (8) it can be verified that the mass transfer resistance is predominantly in the vapour phase. The liquid phase resistance contributes less than 10% of the total resistance; this conclusion was found to be valid for all the six experimental runs carried out in this study.

To understand the phenomena of boundary crossing, consider the component Murphree stage efficiencies, defined by:

$$E_i = \frac{y_{i,L} - y_{i,E}}{y_i^* - y_{i,E}}, \quad i = 1, 2, 3, 4 \quad (20)$$

For the EQ model the component efficiencies are all equal to unity. For the NEQ model the component efficiencies will, in general, differ from one another. This is illustrated by the calculations of E_i for run Q6 in Figure 7(a) obtained from NEQ simulations with a bubble diameter of 5.0 mm. It is clear that the component Murphree efficiencies are all different from one another and vary from stage to stage. In particular it is interesting to note that the methanol efficiency is negative on stage 3. The reason for the negative methanol efficiency is that its constituent driving force is vanishingly small on stage 3 (see Figure 7(b)) and therefore its transfer is dictated by the movement of the other three components in the mixture. The origin of the differences in E_i can be traced to the differences in the binary pair vapour

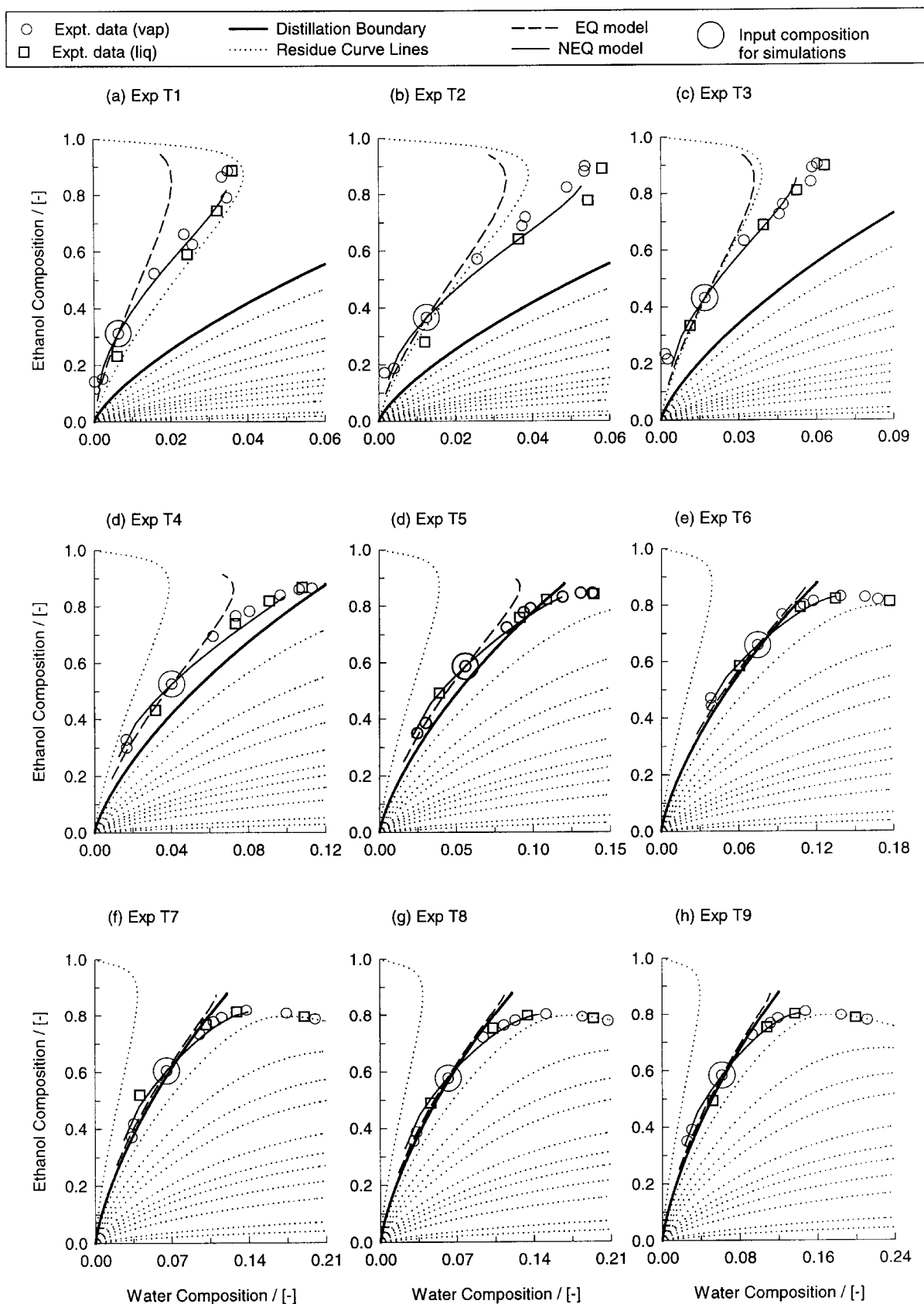


Figure 6. Experimental results (open circles for vapour samples and open squares for liquid samples) showing the column composition trajectories for the water (1)–ethanol (2)–methanol (3) system. Also shown are the simulation results showing the trajectories calculated by the equilibrium (EQ) stage model and the non-equilibrium (NEQ) stage model, along with the residue curve map. The large open circles represent the experimental composition specified in the simulations. In the NEQ model simulations a bubble size $d_b = 5.0$ mm was chosen. The vapour composition leaving stage 4 is used as ‘input’ composition in the simulations.

Table 3. Physical and transport properties for stage 6 of experiment Q6 for the water (1)–ethanol (2)–methanol (3)–acetone (4) system obtained by NEQ model simulations (bubble diameter = 5.0 mm).

Parameter	Units	<i>i-j</i> pair					
		1-2 pair	1-3 pair	1-4 pair	2-3 pair	2-4 pair	3-4 pair
$D_{y,ij}$	$10^{-5} \text{ m}^2 \text{ s}^{-1}$	2.1	2.72	1.82	1.36	0.908	1.18
$D_{x,ij}$	$10^{-9} \text{ m}^2 \text{ s}^{-1}$	6.07	5.52	4.51	4.08	3.07	3.53
$NTU_{y,ij}$	–	1.49	1.93	1.29	0.966	0.644	0.838
$NTU_{x,ij}$	–	16	15.3	13.8	13.1	11.4	12.2
σ	N m^{-1}				0.03357		
ρ_L	kg m^{-3}				771.0		
V_b	m s^{-1}				0.2049		
τ_v	s				0.0449		
Fo_{ij}	–	0.1509	0.1954	0.1308	0.0977	0.0652	0.0848

diffusivities $D_{y,ij}$. If the binary $D_{y,ij}$ were close to one another, the differences in the component efficiencies would be negligible. Differences in the component efficiencies cause the actual composition trajectory followed on any given stage ($y_{i,L} - y_{i,E}$) to deviate from the trajectory dictated by the equilibrium vector ($y_i^* - y_{i,E}$).

For various vapour compositions entering any given stage, the authors have plotted in two ways in Figure 8(a) and (b) the actual composition vector ($y_{i,L} - y_{i,E}$), calculated from the NEQ model (taking bubble diameter of 5.0 mm) along with the equilibrium vector ($y_i^* - y_{i,E}$). The angle

between the NEQ trajectory (continuous line) and the EQ trajectory (dashed line) increases when the differences in the component efficiencies increase. If all the component efficiencies were equal to one another, the NEQ and EQ trajectories would coincide. From Figure 8(b), it can be seen that the NEQ trajectory has a tendency to cut across to the right of the EQ trajectory, precisely as has been observed in the experiments (cf. Figure 3). It is this tendency to cut towards the right of the composition space that causes boundary surface crossing.

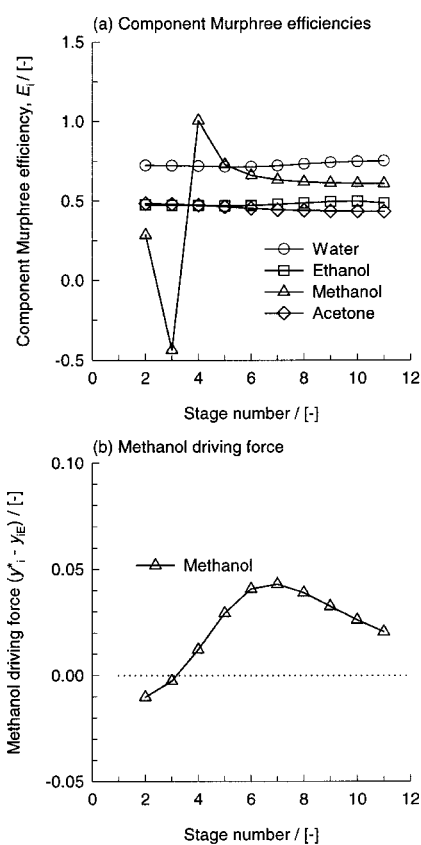


Figure 7. (a) Component efficiencies along the column for the experiment Q6 calculated by the NEQ stage model. In the NEQ model simulations a bubble size $d_b = 5.0$ mm was chosen. (b) Methanol driving force along the column.

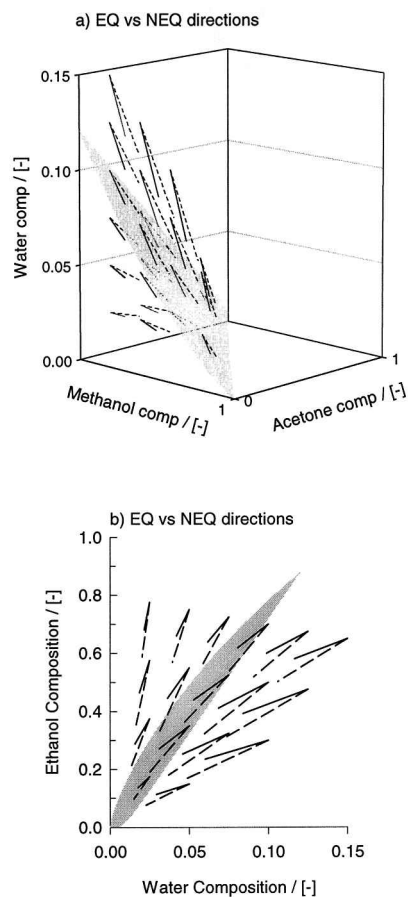


Figure 8. (a-b) Calculated direction vectors using the EQ stage model (100% efficiency for all components, denoted by dashed lines) and the NEQ stage model (denoted by continuous lines). In the NEQ model simulations a bubble size $d_b = 5.0$ mm was chosen.

CONCLUSIONS

The following major conclusions can be drawn from the work presented in this paper.

- (1) The measured composition trajectories during distillation of water–ethanol–methanol–acetone under total reflux conditions in a bubble cap distillation column clearly demonstrate that crossing of a distillation boundary (surface) is possible.
- (2) An NEQ stage model is able to model the experimental results. The experimental results agree very well with the developed model in which a bubble size of 5.0 mm is chosen. The NEQ model correctly anticipates boundary crossing in the quaternary mixture. The choice of bubble size of 5 mm is confirmed by experiments with the ternary mixture water–ethanol–methanol. Here too, boundary crossing is observed in the experiments and this is described by the NEQ model.
- (3) An EQ stage model fails to anticipate boundary crossing in any experiment.
- (4) The differences in the NEQ and EQ trajectories emanates from differences in the component Murphree efficiencies, which in turn can be traced to differences in the binary pair vapour phase diffusivities $\bar{D}_{y,ij}$.

The overall conclusion to be drawn from this work is that for reliable simulation of distillation of azeotropic systems exhibiting a distillation boundary, a rigorous NEQ stage model must be adopted. In a theoretical simulation study, Castillo and Towler³¹ have shown how the differences in the EQ and NEQ distillation column trajectories could be exploited by the engineer in order to obtain process designs that could not be contemplated if mass transfer effects were ignored, and that some designs based solely on EQ models can become infeasible when mass transfer is considered.

NOMENCLATURE

a'	interfacial area per unit volume of vapour bubbles, $\text{m}^2 \text{m}^{-3}$
B_{ij}	NRTL parameters; see Table 1, K
c_i	molar concentration of species i , mol m^{-3}
c_t	mixture molar density, mol m^{-3}
d_b	bubble diameter, m
\bar{D}_{ij}	Maxwell–Stefan diffusivity for pair i – j , $\text{m}^2 \text{s}^{-1}$
E_i^{MV}	component Murphree point efficiency, dimensionless
Fo	fourier number, $Fo \equiv 4\bar{D}_y\tau_v/d_b^2$, dimensionless
G_{ij}	NRTL parameters; see Table 1, dimensionless
g	acceleration due to gravity, m s^{-2}
h	distance along froth height, m
h_f	height of dispersion, m
k_{ij}	element for matrix of multicomponent mass transfer coefficient, m s^{-1}
$[k]$	matrix of multicomponent mass transfer coefficients, m s^{-1}
$[K_{\text{eq}}]$	diagonal matrix of K -values, dimensionless
$[K_{\text{Oy}}]$	matrix of multicomponent overall mass transfer coefficients, m s^{-1}
$[NTU_{\text{Oy}}]$	matrix of overall number of vapour phase transfer units, dimensionless
$[NTU_{\text{Ox}}]$	matrix of overall number of liquid phase transfer units, dimensionless
n	number of diffusing species, dimensionless
$[R_y]$	matrix of inverse mass transfer coefficients, $\text{m}^{-1} \text{s}$
Sh	Sherwood number, dimensionless
t_c	liquid-bubble contact time, s
T	temperature, K
V_b	single bubble rise velocity, m s^{-1}
x_i	liquid composition for component i , dimensionless

y_i	vapour composition for component i , dimensionless
z_i	mole fraction of component i of the appropriate phase, dimensionless

Greek symbols

α_{ij}	non-randomness parameter in NRTL equation, see Table 1, dimensionless
κ_{ij}	binary Maxwell–Stefan mass transfer coefficients, m s^{-1}
ρ_L	density of the liquid, kg m^{-3}
μ_L	liquid viscosity, Pa s
μ_i	molar chemical potential, J mol^{-1}
σ	surface tension, N m^{-1}
τ_v	vapour phase residence time, s
τ_{ij}	NRTL parameters; see Table 1, dimensionless
ζ	dimensionless distance along dispersion or column height, dimensionless

Subscripts

b	referring to a bubble
E	referring to conditions entering a specified stage
f	referring to the froth
i	component number
j	component number
n	component number
L	referring to conditions leaving a specified stage
Oy	overall parameter referred to the vapour phase
ref	reference
t	referring to total mixture
x	referring to the x phase (liquid)
y	referring to the y phase (vapour)

Superscript

M	referring to Murphree
L	referring to the liquid phase
V	referring to the vapour phase
*	referring to equilibrium state

REFERENCES

1. Seader, J. D. and Henley, E. J., 1998, *Separation Process Principles* (John Wiley, New York, USA).
2. *AIChE Bubble Tray Design Manual* (AIChE, New York, USA), 1958.
3. Chan, H. and Fair, J. R., 1983, Prediction of point efficiencies on sieve trays. 1. Binary systems, *Ind Eng Chem Proc Des Dev*, 23: 814–819.
4. Zuiderweg, F. J., 1982, Sieve trays—A view on the state of art, *Chem Eng Sci*, 37: 1441–1461.
5. Rao, D. P., Goutami, C. V. and Jain, S., 2001, A direct method for incorporation of tray-efficiency matrix in simulation of multicomponent separation processes, *Comput Chem Eng*, 25: 1141–1152.
6. Alopaeus, V. and Aittamaa, J., 2000, Appropriate simplifications in calculation of mass transfer in a multicomponent rate-based distillation tray model, *Ind Eng Chem Res*, 39: 4336–4345.
7. Lockett, M. J., 1986, *Distillation Tray Fundamentals* (Cambridge University Press, Cambridge, UK).
8. Stichlmair, J. G. and Fair, J. R., 1998, *Distillation Principles and Practice* (Wiley-VCH, New York, USA).
9. Krishnamurthy, R. and Taylor, R., 1985, Non-equilibrium stage model of multicomponent separation processes, *AIChE J*, 32: 449–465.
10. Taylor, R., Kooijman, H. A. and Hung, J. S., 1994, A second generation non-equilibrium model for computer-simulation of multicomponent separation processes, *Comput Chem Eng*, 18: 205–217.
11. Kooijman, H. A. and Taylor, R., 2001, *The Chem Sep Book* (Libri Books, Books on Demand, Norderstedt, Germany), www.chemsep.org.
12. Agarwal, S. and Taylor, R., 1994, Distillation column design calculations using a non-equilibrium model, *Ind Eng Chem Res*, 33: 2631–2636.
13. Taylor, R. and Krishna, R., 1993, *Multicomponent Mass Transfer* (John Wiley, New York, USA).
14. Krishna, R. and Wesselingh, J. A., 1997, The Maxwell–Stefan approach to mass transfer, *Chem Eng Sci*, 52: 861–911.
15. Wesselingh, J. A. and Krishna, R., 2000, *Mass Transfer in Multicomponent Mixtures* (Delft University Press, Delft, The Netherlands).
16. Pagani, G., Monforte, A. A. and Bianchi, G., 2001, Transfer-based models implementation in an equation oriented package, *Comput Chem Eng*, 25: 1493–1511.
17. Muller, N. P. and Segura, H., 2000, An overall rate-based stage model for cross flow distillation columns, *Chem Eng Sci*, 55: 2515–2528.

18. Higler, A., Krishna, R. and Taylor, R., 1999, A non-equilibrium cell model for packed distillation columns. The influence of maldistribution, *Ind Eng Chem Res*, **38**, 3988–3999.
19. Eckert, E. and Vanek, T., 2001, Some aspects of rate-based modelling and simulation of three-phase distillation columns, *Comput Chem Eng*, **25**: 603–612.
20. Pacheco, M. A. and Rochelle, G. T., 1998, Rate based modelling of reactive absorption of CO₂ and H₂S into aqueous methyldiethanolamine, *Ind Eng Chem Res*, **37**: 4107–4117.
21. Taylor, R. and Krishna, R., 2000, Modelling reactive distillation, *Chem Eng Sci*, **55**: 5183–5229.
22. Baur, R., Taylor, R., Krishna, R. and Copati, J. A., 1999, Influence of mass transfer in distillation of mixtures with a distillation boundary, *Trans IChemE, Part A, Chem Eng Res Des*, **77**: 561–565.
23. Springer, P. A. M. and Krishna, R., 2001, Crossing of boundaries in ternary azeotropic distillation: Influence of interphase mass transfer, *Int Commun Heat Mass*, **28**: 347–356.
24. Pelkonen, S., Kaesemann, R. and Gorak, A., 1997, Distillation lines for multicomponent separation in packed columns: Theory and comparison with experiment, *Ind Eng Chem Res*, **36**: 5392–5398.
25. Pelkonen, S., Górak, A., Ohligschläger, A. and Kaesemann, R., 2001, Experimental study on multicomponent distillation in packed columns, *Chem Eng Process*, **40**: 235–243.
26. Springer, P. A. M., Buttinger, B., Baur, R. and Krishna, R., 2002, Crossing of distillation boundary in homogeneous azeotropic distillation: Influence of interphase mass transfer, *Ind Eng Chem Res*, **41**: 1621–1631.
27. Doherty, M. F. and Malone, M. F., 2001, *Conceptual Design of Distillation Systems* (McGraw-Hill, New York, USA).
28. Gmehling, J. L. and Onken, U., 1977, *Vapour-Liquid Equilibrium Data Collection* (Dechema, Frankfurt, Germany).
29. Mendelson, H. D., 1967, The prediction of bubble terminal velocities from wave theory, *AIChE J*, **13**: 250–253.
30. Krishna, R., Urseanu, M. I., van Baten, J. M. and Ellenberger, J., 1999, Wall effects on the rise of single gas bubbles in liquids, *Int Commun Heat Mass*, **26**: 781–790.
31. Castillo, F. J. L. and Towler, G. P., 1998, Influence of multicomponent mass transfer on homogeneous azeotropic distillation, *Chem Eng Sci*, **53**: 963–976.

ACKNOWLEDGEMENTS

The authors acknowledge a grant from the Netherlands Organization for Scientific Research (NWO), Chemical Sciences Division (CW), for investigations on three-phase distillation. The authors are grateful to R. Taylor and H. Kooijman for providing the code to *ChemSep*, which was used in this study after appropriate modification to include the rigid bubble model. R.K. dedicates this paper to Prof. J. A. Wesselingh, a staunch champion of the Maxwell–Stefan approach, as felicitation on his 65th birthday in 2002.

ADDRESS

Correspondence concerning this paper should be addressed to Professor R. Krishna, Department of Chemical Engineering, University of Amsterdam, Nieuwe Achtergracht 166, 1018 WV, Amsterdam, The Netherlands. E-mail: krishna@science.uva.nl

The manuscript was communicated via our International Editor for The Netherlands, Professor P. Jansens. It was received on 24 January 2002 and accepted for publication after revision 11 April 2002.